CATENOID IN AN ELECTRIC FIELD

D.E. MOULTON* AND J.A. PELESKO†

Abstract. Mathematical models of electrostatic actuation have been developed since the 1960's, beginning with the work of G.I. Taylor, and are of great utility in a number of engineering systems. They are of particular use in the field of micro- and nanoelectromechanical systems, where models have typically dealt with planar geometries. Here, we extend the theory of electrostatic actuation to a non-planar geometry by studying a catenoid soap-film bridge placed in an axially symmetric electric field. A model is formulated and analyzed, with emphasis on stability and the effect of dimensionless parameters. In the absence of external forces, the catenoid assumes its shape driven by surface tension. The utility of adding electrostatic forces and the interaction with surface tension is examined. Specifically, we uncover and quantify a stabilizing effect of the electric field and explore the limit of the stabilization.

Key words. minimal surface, MEMS, microelectromechanical systems, mean curvature, capillary surface, stabilization

AMS subject classifications. 34, 35, 74, 78

1. Introduction. In the late 1960's, G.I. Taylor launched the field of electrohydrodynamics through a series of pioneering studies [12]. Of special note is [12], where Taylor studied the electrostatic deflection of planar soap films. While Taylor's intent was to shed light on the coalescence of raindrops in electrified clouds, the last fifty years have shown that Taylor's simple system is in fact of great technological importance. Today, researchers studying engineering technologies such as micro- and nanoelectromechanical systems (MEMS and NEMS) [9], self-assembly [5], and electrospinning [8] all point to Taylor's work as a seminal contribution to their fields.

Perhaps the most direct application of Taylor's soap film study has been in the field of MEMS and NEMS. Here, researchers have developed a variety of devices such as grating light valves, micromirrors, comb drives, and micropumps, that operate based on the principle of electrostatic actuation explored by Taylor. All of these systems operate in essentially the same way; a voltage difference is applied between mechanical components of the system, this voltage difference induces a Coulomb force between the components, and, in turn, these components deform in the presence of this force. In the Taylor system, the mechanical components were a pair of planar soap films and Taylor studied their deflection under the influence of the Coulomb force.

Driven by typical features of MEMS devices, models of electrostatic actuation have generally dealt with planar components [9, 3]. Recent developments, especially in the field of self-assembly, indicate that it is time to push beyond the planar level to more complex geometries. Perhaps the clearest example of this need lies in the experimental work of Whitesides, [5]. In attempting to develop new fabrication technologies for MEMS and NEMS, Whitesides explored a form of self-assembly based on the tendency of systems to minimize surface energy. In particular, Whitesides placed drops of polydimethylsiloxane (PDMS) between two rigid plates. These droplets naturally form a "liquid bridge." By adjusting the gap between the plates and the relative orientation of the plates, a variety of structures can be formed. In the PDMS system,

*Corresponding Author, University of Arizona, Department of Mathematics, Tucson, AZ (moulton@math.arizona.edu)

†University of Delaware, Department of Mathematical Sciences, Newark, DE (pelesko@math.udel.edu).

the polymer can be cross-linked, solidifying the liquid bridge and hence leading to the production of small components with a variety of shapes. In [5], Whitesides notes that a much greater range of shapes could be formed if the bridges were manipulated with an electric field.

In this paper, we take a first step in this direction through the study of a catenoid shaped membrane, i.e., a simple minimal surface, placed in an electric field. It is useful to contrast the model developed here with typical models of electrostatic actuation. The governing equation that we will derive has the general form

$$Hu = f(u) \,, \tag{1.1}$$

where the function u gives the radial coordinate of a deflected surface of revolution. Here, H is the mean curvature operator, and the function $f(u)$ captures the Coulomb force due to the presence of the electric field. Typical models of electrostatic actuation have the general form

$$\Delta u = g(u) \,, \tag{1.2}$$

where again, u measures the deflection of some surface, and $g(u)$ captures the Coulomb force. Note that moving to a more general geometry implies that the mean curvature operator, H, cannot be linearized and replaced by the Laplacian as in Equation (1.2). Also note that $g(u)$ typically contains a simple inverse square non-linearity, while here we are forced to deal with a more intractable logarithmic non-linearity in $f(u)$.

It is also worthwhile to note that our basic model, Equation (1.1), connects the theory of electrostatic actuation to the theory of minimal surfaces, [10], and the theory of constant mean curvature surfaces, [1]. In Equation (1.1), if $f(u)$ is set to zero, we are studying a minimal surface. In this study, the "base case," occurring when the electric field is turned off, is the well-known catenoid minimal surface. On the other hand, when $f(u)$ is constant, Equation (1.1), becomes the basic equation studied in the field of constant mean curvature or capillary surfaces. The dependence here of $f(u)$ on the shape of the surface studied and the fact that it arises due to the presence of an electric field, leads us to suggest the designation "Field Driven Mean Curvature Surface" (FDMC) for surfaces satisfying Equation (1.1).

In this paper we begin in Section 2 by deriving the governing equations for a catenoid shaped elastic membrane, i.e., a soap film, placed in the presence of an electric field. We take a variational approach to deriving the governing equations and simplify the model through the use of asymptotic analysis. Next, in Section 3, we analyze Equation (1.1) for our geometry using dynamical systems techniques. In Section 4, we turn to perturbation methods and perform an analysis of the special cases of small voltage and a nearly cylindrical surface. In Section 5, we address stability and connect the analyses of Sections 3 and 4 while exploring a peculiar instability relationship.

2. Formulation of the Model. In this section we present the governing equations for our electrostatically actuated membrane. The system we study consists of two parallel rings of radius a with a thin elastic conducting membrane forming a bridge between the rings. We take the distance between the rings to be L. Surrounding the rings is a uniform perfectly conducting cylinder of radius b with $b > a$. The top and bottom of the apparatus are left open, and there is no direct connection between the rings and the outer cylinder. A potential difference is applied between the membrane and the outer cylinder. We take the outer cylinder to have potential V and the membrane to have zero potential. The geometry is sketched in Figure 2.1.

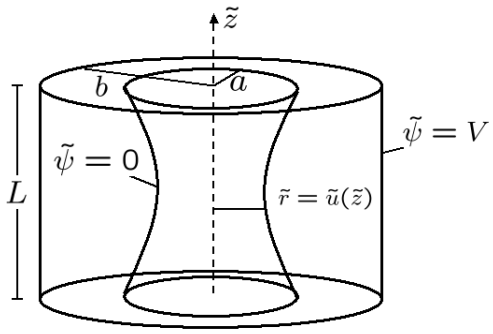

FIG. 2.1. *The basic setup for the problem.*

We begin by formulating the equations governing the electric field. Denoting the electrostatic potential by $\tilde{\psi}$ and working in cylindrical coordinates, $\tilde{\psi}(\tilde{r}, \theta, \tilde{z})$ satisfies

$$\Delta\tilde{\psi} = 0, \quad \tilde{\psi}(b, \theta, \tilde{z}) = V, \quad \tilde{\psi}(\tilde{u}(\tilde{z}), \theta, \tilde{z}) = 0 \,, \tag{2.1}$$

where $\tilde{r} = \tilde{u}(\tilde{z})$ defines the membrane surface. Note that we are assuming axial symmetry so that $\tilde{u}$ depends only on $\tilde{z}$; the membrane is a surface of revolution.

Next, we introduce the non-dimensional variables

$$z = \frac{\tilde{z}}{L}, \quad r = \frac{\tilde{r}}{b-a}, \quad \psi = \frac{\tilde{\psi}}{V}, \quad u = \frac{\tilde{u}}{a} \,. \tag{2.2}$$

Making these substitutions in Equations (2.1), we obtain

$$\begin{aligned} &\frac{\partial^2\psi}{\partial r^2} + \frac{1}{r}\frac{\partial\psi}{\partial r} + \epsilon^2\frac{\partial^2\psi}{\partial z^2} = 0 \\ &\psi = 1 \ \text{ at } r = \frac{b}{b-a}, \quad \psi = 0 \ \text{ at } r = u(z)\frac{a}{b-a} \,. \end{aligned} \tag{2.3}$$

Here, $\epsilon = (b-a)/L$ is a dimensionless aspect ratio comparing the gap size between the rings and the outer cylinder to the length of the device. We assume $\epsilon^2 << 1$. The electrostatic field energy is given in dimensional form by

$$-\frac{\epsilon_0}{2}\int |\nabla\tilde{\psi}|^2 \,, \tag{2.4}$$

where the integral is taken over the region between the outer cylinder and the membrane, and ϵ_0 is the permittivity of free space. The elastic energy is the product of surface tension T and the surface area of the membrane; the total energy is the sum of the elastic and electrostatic energies. Upon solving Equations (2.3) after dropping the ϵ^2 term, and after using the divergence theorem, we obtain the dimensionless energy functional

$$\mathcal{E}[u] = \int_{-1/2}^{1/2} u\sqrt{1+\sigma^2 u'^2} - \frac{\lambda}{\ln(\delta/u)}\, dz\ , \tag{2.5}$$

where $\delta = b/a$ is the ratio of the radii of the inner and outer cylinders, $\sigma = a/L$ is the ratio of the inner radius to the length, and $\lambda = \epsilon_0 V^2/(2Ta)$ is a dimensionless variable characterizing the relative strengths of electrostatic and mechanical forces in the problem. We may think of λ as a control parameter related to the voltage. Note that although we have introduced four dimensionless parameters, there are in fact only three *independent* parameters. The parameters ϵ, σ, and δ are all related by $\epsilon = \sigma(\delta - 1)$. We use these four parameters for convenience of notation, while keeping in mind that the range of σ and δ is limited by our assumption that $\epsilon^2 << 1$. Note also that primes denote differentiation with respect to z. We minimize the energy $\mathcal{E}$ by taking a first variational derivative and obtain the following ODE for the shape of the membrane $u(z)$

$$\frac{1+\sigma^2 u'^2 - \sigma^2 u u''}{(1+\sigma^2 u'^2)^{3/2}} = \frac{\lambda}{u\ln^2(\delta/u)}\ . \tag{2.6}$$

To complete the system, we impose the boundary condition that requires that the membrane be connected to the rings, expressed in dimensionless form as

$$u(1/2) = u(-1/2) = 1\ . \tag{2.7}$$

Equations (2.6) - (2.7) govern the equilibrium shape of the deflected membrane. Note that the left hand side of Equation (2.6) is the mean curvature, while the right hand side contains the effect of the electric field. Our goal is to determine the solution set to this boundary value problem, to explore stability and multiplicity of solutions, and to understand the solution set in terms of the parameters λ, σ, and δ.

3. Phase plane analysis. We begin our analysis of the BVP (2.6) - (2.7) by considering the nature of trajectories in the phase plane. Rewriting the ODE (2.6) as a first order system, we have

$$\begin{aligned} u' &= v \\ v' &= \frac{1+\sigma^2 v^2}{\sigma^2 u} - \frac{\lambda(1+\sigma^2 v^2)^{3/2}}{\sigma^2 u^2 \ln^2(\delta/u)}\ . \end{aligned} \tag{3.1}$$

The critical points for this system are located at $v = 0$, and solutions of $u\ln^2(\delta/u) = \lambda$. For a given λ, there are 2 solutions, meaning that there are 2 critical points, which we denote $(u^*_{(1)}, 0)$ and $(u^*_{(2)}, 0)$, with $u^*_{(1)} < u^*_{(2)}$. These points coalesce as λ tends to $4\delta/e^2$. If $\lambda > 4\delta/e^2$, there are no critical points for the system.

For $\lambda < 4\delta/e^2$, linear stability analysis shows that $(u^*_{(1)}, 0)$ is a saddle node, while $(u^*_{(2)}, 0)$ is a center. See Figure 3.1 for a sample phase portrait. Note that the system (3.1) is unaltered by the change of variables $v \mapsto -v$, $z \mapsto -z$. This symmetry means that the trajectories in the lower half plane are the same as in the upper half but with

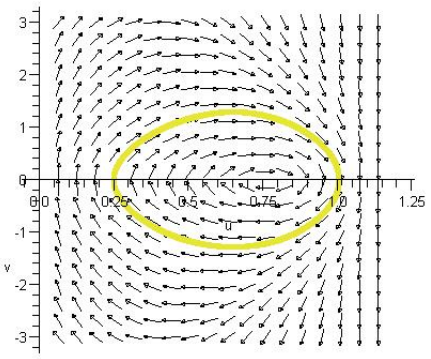

FIG. 3.1. *Phase plane plot in the $u - v$ plane, for $\lambda = .15, \sigma = 1, \delta = 1.2$. There are 2 critical points: a saddle point located approx. at $(.004, 0)$, and a center at approx $(.77, 0)$. A sample trajectory is included*

the direction reversed, which is evident in Figure 3.1. This symmetry allows us to conclude that the right critical point is indeed a center [11].

Note that v' blows up at $u = 0$ and $u = \delta$. However, solutions to Equations (2.6) – (2.7) are entirely contained within $0 < u < \delta$. The case $u = 0$ corresponds to self-intersection of the membrane. The case $u = \delta$ corresponds to the membrane touching the outer cylinder. These are the physical bounds for the problem, so we restrict our attention to $u \in (0, \delta)$.

As is proved in [7], the phase plane contains a homoclinic orbit. The orbit departs from the left critical point $(u^*_{(1)}, 0)$, circles the right critical point $(u^*_{(2)}, 0)$, and returns to $(u^*_{(1)}, 0)$ as $z \to \infty$. This divides the phase plane into two regions. Inside the homoclinic orbit, all trajectories are periodic, circling the critical point $(u^*_{(2)}, 0)$. Outside the orbit trajectories are non-periodic and approach $v = \pm\infty$.

To be a solution to the boundary value problem, a trajectory in the phase plane must start on the vertical line $u = 1$, and return to this line after a time of flight of 1. The trajectory may wrap around any number of times, which will dictate the shape of the solution. Figure 3.2 depicts some potential solution trajectories and the resultant membrane surfaces they define.

As is evident in Figure 3.2, there is a potential for a high number of solutions to the BVP. Most of the these solutions are highly oscillatory and physically unstable [7]. On the other hand, from a mathematical point of view, there is value in characterizing the overall structure of the full solution set. Our analysis in this section is directed towards this aim. To this end, we approach the problem by defining time of flight integrals for trajectories. In this paper, we will only consider solutions which are symmetric about the midplane $z = 0$. An analysis of non-symmetric solutions is found in [7]. Under this symmetry assumption, we classify a solution as a trajectory that begins on the axis $v = 0$ and ends on the line $u = 1$ after a time of flight of $1/2$. Applying the Beltrami identity [13] to the energy functional Equation (2.5) enables us to obtain the following first integral of Equation (2.6)

$$\frac{u}{\sqrt{1 + \sigma^2 u'^2}} - \frac{\lambda}{\ln(\delta/u)} = E \, . \tag{3.2}$$

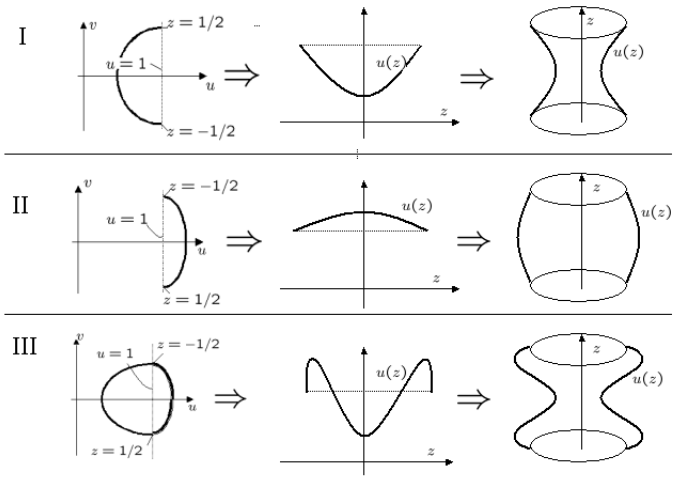

FIG. 3.2. *Depiction of solution trajectories in the phase plane and the resulting solution curves and membrane surfaces.*

Here the constant E represents a conserved quantity in the system. Setting $z = 0$ and using $u'(0) = 0$, we find

$$E = u_0 - \frac{\lambda}{\ln(\delta/u_0)} \,, \tag{3.3}$$

where $u_0 = u(0)$. Solving Equation (3.2) for u', we have

$$u' = \frac{1}{\sigma}\left\{\left(\frac{u}{E + \frac{\lambda}{\ln(\delta/u)}}\right)^2 - 1\right\}^{1/2} \,. \tag{3.4}$$

Note that in solving for u', symmetry allows us to take the positive square root without loss of generality. Denote the right hand side of Equation (3.4) by $f(u; u_0)$. Separating variables, we obtain

$$z = \int_{u_0}^{u(z)} \frac{du}{f(u; u_0)} \,. \tag{3.5}$$

A solution must satisfy $u(1/2) = 1$, which would lead us to require

$$\int_{u_0}^{1} \frac{du}{f(u; u_0)} = 1/2 \,. \tag{3.6}$$

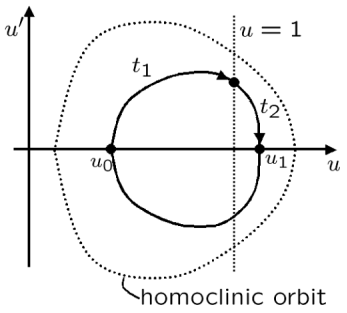

FIG. 3.3. *The values t_1 and t_2 for trajectories inside the homoclinic orbit.*

However, this is not sufficient, as we will not catch trajectories that "wrap around" in time of flight 1/2 before ending on the line $u = 1$, for in these cases the domain of the integrand is not well defined in the integral. See, for instance, Example III in Figure 3.2. Such a trajectory can only occur inside the homoclinic orbit, so for the time being we restrict our attention to this region.

We begin with trajectories for which $u_0 = u(0) < 1$. Consider Figure 3.3. In order to verify whether a trajectory inside the homoclinic orbit is a solution or not, all we need to know are the values t_1 and t_2, which represent the time it takes the trajectory to travel from the u-axis to the line $u = 1$ and the time it takes to go from this line back to the axis, respectively. In particular, if $t_1 = 1/2$, we have a simple monotonic solution (on the interval $[0, 1/2]$), as depicted in Example I of Figure 3.2. In general, a solution will satisfy

$$\begin{gathered}(2k+1)t_1 + (2k)t_2 = 1/2 \\ \text{or} \\ (2k+1)t_1 + (2k+2)t_2 = 1/2, \quad k \in \mathbb{N}_0 \, .\end{gathered} \tag{3.7}$$

These combinations account for every possible way that a trajectory may begin on the line $v = 0$ with $u < 1$ and end on the line $u = 1$ after a time of flight of 1/2. The value of the non-negative integer k signifies the number of times the trajectory will circle around in the phase plane in time of flight 1/2, and thus the number of oscillations in the solution curve. The larger k is, the more oscillatory the solution. Hence, we refer to k as describing the mode of the solution.

To find the values t_1 and t_2, we need the corresponding u value where the trajectory intersects the u-axis (see Figure 3.3). Denoting this by u_1, we see that u_1 must satisfy $f(u_1; u_0) = 0$, since $u' = f(u; u_0)$. This implies

$$u_1 = E + \frac{\lambda}{\ln(\delta/u_1)} \, ,$$

where E is defined by u_0. Referring to Equation (3.5), we have

$$t_1(u_0) = \int_{u_0}^{1} \frac{du}{f(u; u_0)}, \;\; t_2(u_0) = \int_{1}^{u_1} \frac{du}{f(u; u_0)} \, . \tag{3.8}$$

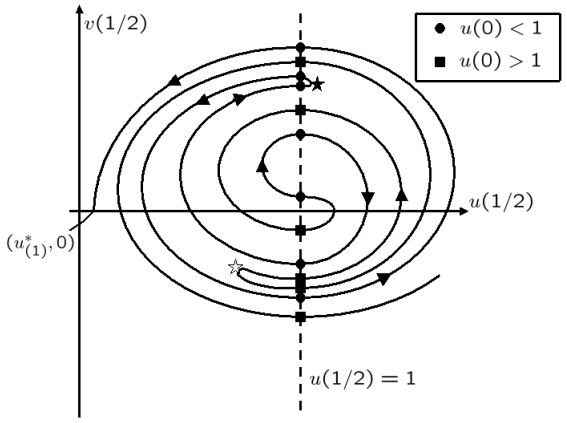

FIG. 3.4. *Cartoon depiction of the spiral meander inside the homoclinic orbit, with the scaling toward the edge of the homoclinic orbit blown up for clarity. Each intersection with the line* $u(1/2) = 1$ *represents a solution. The type of solution is indicated. The arrows indicate the direction of decreasing* u_0.

For trajectories that satisfy $u_0 = u(0) > 1$, we need merely interchange the roles of t_1 and t_2 in the above analysis. In principle, if we find the values t_1 and t_2 for all values of u_0, we may use the criteria of Equations (3.7) to determine the location and mode of all solutions as well as determine the total number of solutions for a given parameter set.

Casting the problem in terms of the t_i enables us to determine the structure of the solution set. To visualize this, in Figure 3.4 we plot a meander for the BVP [2]. In this approach, we choose a starting point $u(0)$ with $v(0) = 0$, integrate from $z = 0$ to $z = 1/2$, and plot the resulting point $(u(1/2),\ v(1/2))$. In this manner, ranging through all starting points $u(0)$ inside the homoclinic orbit, we may plot a curve in the $(u(1/2),\ v(1/2))$ plane parameterized by $u(0)$. Every intersection with the line $u(1/2) = 1$ represents a solution to the BVP.

Due to difficulties with numerical integration, Figure 3.4 is a cartoon depiction of the spiral meander inside the homoclinic orbit, produced by studying the nature of the integrals t_i. A detailed analysis of this spiral structure is provided in [7]. We present it here to demonstrate the rich solution structure present for the BVP.

4. Special solutions - asymptotic analysis. In this section, we investigate two special solutions, the catenoid that appears when there is zero voltage, and the cylindrical solution. We develop asymptotic schemes to explore perturbations from these solutions and to understand their dependence on the parameters.

4.1. Small voltage case. First, we examine the case of small voltage. Suppose there is zero voltage. Eliminating the electric field reduces the problem to that of a thin membrane bridging two parallel rings. Setting $\lambda = 0$ in Equation (2.6), $u(z)$ must have zero mean curvature; that is, the membrane should be a minimal surface. This problem has the well-known catenoid solution defined by

$$u(z) = \frac{\cosh(c_2 z)}{c_2 \sigma}\ , \tag{4.1}$$

where c_2 is a constant satisfying

$$\sigma = \frac{\cosh(c_2/2)}{c_2} \ . \tag{4.2}$$

For certain values of σ, there are two values of c_2 that satisfy Equation (4.2), and so two catenoid solutions. The smaller value of c_2 corresponds to a stable catenoid, while the other value corresponds to an unstable solution. The range for which a solution exists is given approximately by $\sigma \geq 0.7545$. Denote this critical value by σ_{cr}. The fact that the catenoid ceases to exist beyond this is tantamount to the observation that if you pull the two rings too far apart (i.e. increase the L in $\sigma = a/L$), you reach a point where the membrane pinches off and separates.

With the solutions of zero voltage in mind, we consider the case of small voltage, and look for perturbations from the catenoid solutions. To do this, we assume that $\lambda << 1$, and that $u(z)$ can be expanded as

$$u \sim u_0 + \lambda u_1 + \lambda^2 u_2 + \cdots \tag{4.3}$$

Before we proceed, recall that in deriving the energy functional, we used the small aspect ratio assumption $\epsilon^2 << 1$ in order to solve for the electric potential to leading order. In order for the current asymptotic analyis to be compatible with this, we must assume that $\epsilon^2 = o(\lambda)$. In other words, in implicitly deriving the energy functional from a first order expansion in ϵ^2, we must clarify that the other parameters in the problem are bigger than ϵ^2.

Under this assumption, we insert the expansion (4.3) into Equation (2.6) and collect like powers of λ. We obtain as a leading order solution the catenoid given by Equation (4.1). At $O(\lambda)$, we have

$$u_1{}'' - 2c_2 \tanh(c_2 z) u_1{}' + c_2^2 u_1 = \frac{-(1+\sigma^2 u_0^2)^{3/2}}{\sigma^2 u_0^2 \ln^2(\delta/u_0)} \tag{4.4}$$

along with boundary conditions $u_1(1/2) = u_1(-1/2) = 0$. Setting the right hand side of Equation (4.4) to zero, the homogeneous solution is found to be

$$u_1^h(z) = A\sinh(c_2 z) + B(c_2 z \sinh(c_2 z) - \cosh(c_2 z)) \ , \tag{4.5}$$

where A and B are constants. The boundary conditions can only be met for the c_2, σ pair at the critical value σ_{cr}. Therefore, if $\sigma > \sigma_{cr}$, the non-homogeneous problem Equation (4.4) will have a solution. Actually, for such a σ, we have two solutions, as there are two valid c_2 values. We have a perturbation from the stable catenoid as well as a perturbation from the unstable catenoid. These solutions may by found using variation of parameters. For the stable catenoid perturbation, increasing λ causes the membrane to deflect out toward the outer cylinder as the voltage is increased. With the unstable catenoid perturbation, the opposite occurs. In problems of electrostatic deflection, it is typical that a stable solution deflects toward the source of the applied voltage while an unstable solution deflects in the opposite direction. See, for instance, [9].

If $\sigma = \sigma_{cr}$, the homogeneous problem will have a solution, u_1^h, and the criteria for there to be a solution to Equation (4.4) is that

$$\int_{-1/2}^{1/2} \frac{(1+\sigma^2 u_0'^2)^{3/2}}{u_0^2 \ln(\delta/u_0)^2} \cdot u_1^h \, dz = 0 \, . \tag{4.6}$$

It is easily shown that u_1^h carries only one sign in the interval $[-1/2, 1/2]$, and so the integral cannot vanish. Thus, our asymptotic expansion fails when $\sigma = \sigma_{cr}$. To fix this, we need to modify our assumption on the ordering of the expansion. If we instead take

$$u \sim u_0 + \lambda^{1/2} u_1 + \lambda u_2 + \ldots$$

we arrive at the same leading order solution u_0 given by Equation (4.1), but here there is only one value of c_2 and thus one u_0 solution since $\sigma = \sigma_{cr}$. In this case, the $O(\lambda^{1/2})$ problem is the same as before, but now with zero right hand side. We express this problem by defining a new operator L as follows:

$$L[u] := u'' - 2\tanh(c_2 z)u' + c_2^2 u \, . \tag{4.7}$$

In terms of this operator, u_1 satisfies $L[u_1] = 0$ with zero boundary data. Since we are at the critical σ value, this problem has a solution, given by

$$u_1 = B \cdot (c_2 z \sinh(c_2 z) - \cosh(c_2 z)) \, .$$

The constant B is undetermined, as one boundary condition is automatically satisfied. To determine B, we go to the $O(\lambda)$ problem, which may be written

$$L[u_2] = -\frac{(1+\sigma^2 u_0'^2)^{3/2}}{\sigma^2 u_0^2 \ln(\delta/u_0)^2} + \frac{u_1'^2}{u_0} - \frac{u_1 u_1''}{u_0} \, . \tag{4.8}$$

Everything on the right hand side of Equation (4.8) is fixed except for the unknown constant B in u_1. Denote the right hand side as $G(B)$. The solvability condition for u_2 is

$$\int_{-1/2}^{1/2} G(B) u_2^h \, dz = 0 \, , \tag{4.9}$$

where u_2^h is the homogeneous solution to Equation (4.8). However, u_2^h will only differ by a constant from u_1. Thus, Equation (4.9) gives us a condition for finding B. We may find this explicitly if we introduce the function $\hat{u} = c_2 z \sinh(c_2 z) - \cosh(c_2 z)$ so that $u_1 = B\hat{u}$. From Equation (4.9), we may solve to find

$$B^2 = \frac{\displaystyle\int_{-1/2}^{1/2} \frac{\hat{u}(1+\sigma_{cr}^2 u_0'^2)^{3/2}}{\sigma_{cr}^2 u_0^2 \ln(\delta/u_0)^2} \, dz}{\displaystyle\int_{-1/2}^{1/2} \frac{\hat{u}\hat{u}'^2 - \hat{u}^2\hat{u}''}{u_0} \, dz} \, . \tag{4.10}$$

The right hand side of Equation (4.10) is completely determined for fixed δ, and is found to be positive. Accordingly, there are two possible values for B, and so two solutions at $\sigma = \sigma_{cr}$. This is not surprising. Recall that σ_{cr} defines the bifurcation length for the stable and unstable catenoids with zero voltage. By applying the electric field, we have added a force counter to the surface tension which is pulling the membrane in. We should expect that the membrane is able to be stabilized at lengths greater than occur without any applied voltage. In other words, with small voltage, we see that the bifurcation point will occur for a smaller value of σ, i.e., a greater length, than with no voltage.

When will the bifurcation occur? To answer this, we return to the expansion and again assume small voltage, but take $\sigma < \sigma_{cr}$, so that the length is greater than the critical zero voltage length. More precisely, we assume

$$\sigma^2 = \sigma_{cr}^2 - \gamma\lambda, \quad u \sim u_0 + \lambda^{1/2}u_1 + \lambda u_2 + \cdots \tag{4.11}$$

where $\gamma > 0$ is to be determined. We find again that $u_0 = \cosh(c_2 z)/(\sigma_{cr}c_2)$ is the zero voltage bifurcation catenoid. In this case, we have $L[u_1] = 0$, implying as before that $u_1 = B\hat{u}$ where B is yet to be determined. At $O(\lambda)$, we find that

$$L[u_2] = -\frac{(1+\sigma_{cr}^2 u_0'^2)^{3/2}}{\sigma_{cr}^2 u_0^2 \ln^2(\delta/u_0)} - \frac{u_1 u_1''}{u_0} + \frac{u_1'^2}{u_0} - \gamma\left(\frac{u_0'^2 - u_0 u_0''}{\sigma_{cr}^2 u_0}\right) . \tag{4.12}$$

Denote the right hand side of Equation (4.12) by $G(B, \gamma)$. In this case, the orthogonality condition gives us a relationship between B and γ. After some simplification, this relationship may be expressed as

$$B^2 I_1 - I_2 = \gamma I_3 , \tag{4.13}$$

where the values $I_k,\ k = 1, 2, 3$ are explicitly defined by

$$\begin{aligned} I_1 &= \int_{-1/2}^{1/2} \frac{\hat{u}\hat{u}'^2 - \hat{u}^2\hat{u}''}{u_0}\, dz, \quad I_2 = \int_{-1/2}^{1/2} \frac{\hat{u}(1+\sigma_{cr}^2 u_0'^2)^{3/2}}{\sigma_{cr}^2 u_0^2 \ln^2(\delta/u_0)}\, dz, \\ I_3 &= \int_{-1/2}^{1/2} \frac{\hat{u}(u_0'^2 - u_0 u_0'')}{\sigma_{cr}^2 u_0}\, dz . \end{aligned} \tag{4.14}$$

Note that $I_1 \approx -10.248,\ \ I_3 \approx 3.459$ are fixed values, while I_2 depends on δ but will always be negative.

Suppose that we have fixed $\sigma < \sigma_{cr}$ and have fixed $\lambda << 1$. Then, recalling the relationship $\sigma^2 = \sigma_{cr}^2 - \gamma\lambda^\beta$, we have also fixed γ (noting that $\beta = 1$). We may solve Equation (4.13) for B, finding two possible solutions representing the perturbations from the stable and unstable catenoids. This will only work if the term within the square root is positive when solving for B. Thus, Equation (4.13) enables us to approximate the critical length at which the bifurcation between the two perturbed catenoids occurs. In view of the signs of the integrals I_k in Equation (4.14), the

bifurcation between the two solutions occurs when $\gamma = \frac{-I_2}{I_3}$, and so the critical value of σ is

$$\sigma^* = \left(\sigma_{cr}^2 + \frac{I_2\lambda}{I_3}\right)^{1/2} . \tag{4.15}$$

For clarity, note that we use σ^* here to denote the critical length ratio when the voltage is on, whereas σ_{cr} is the critical length ratio of zero voltage.

4.2. Cylinder solution. In this section, we consider the constant solution $u = 1$. Observe from Equation (2.6) that this solution occurs for $\lambda = \ln^2 \delta$. Physically, this represents the membrane forming a cylindrical bridge. To investigate perturbations from the cylinder, let

$$\lambda = \ln^2 \delta + \nu, \quad u \sim 1 + \nu u_1 + \nu^2 u_2 + \ldots, \quad \nu << 1 \tag{4.16}$$

As before, we need to compare the size of ν with ϵ. Here, the requirement is that $\nu << \ln^2(1 + \epsilon/\sigma)$, which relates the fact that the perturbation should be smaller than the voltage we are perturbing from.

Inserting the expansion (4.16) into the ODE (2.6), we obtain the $O(\nu)$ problem

$$\begin{aligned} &u_1'' + \mu^2 u_1 = -A \\ &u_1(-1/2) = 0, \;\; u_1(1/2) = 0 \, , \end{aligned} \tag{4.17}$$

where

$$\mu^2 = \frac{2 - \ln\delta}{\sigma^2 \ln\delta}, \quad A = \frac{1}{\sigma^2 \ln^2 \delta} \, . \tag{4.18}$$

Note that $\mu^2 > 0$ if $\delta < e^2$. In this case, the solution is found to be

$$u_1 = \frac{A}{\mu^2}\left(\frac{\cos(\mu z)}{\cos(\mu/2)} - 1\right) \, . \tag{4.19}$$

If $\delta = e^2$, we get parabolic solutions, and $\delta > e^2$ leads to hyperbolic solutions. However, based on our previous ordering arguments, $\delta < e^2$ is the physically relevant parameter range, and so we restrict our analysis to this set. Note that the solution does not exist when $\mu = (2n + 1)\pi$ for integers n. This is fixed by altering our expansion and using solvability arguments similar to those used in the case of the catenoid perturbation. Details are found in [7]. The conclusion of this analysis is that when μ is equal to an odd multiple of π:

- There are two solutions symmetric about the line $u = 1$ when the voltage is less than the cylinder voltage, i.e. for $\lambda < \ln^2 \delta$.
- As λ is increased to $\ln^2 \delta$, these two solutions coalesce into the cylinder solution, and so taking any $\lambda > \ln^2 \delta$ yields no solution.

5. Stability. When $\lambda = 0$, $\sigma* = \sigma_{cr} \approx 0.7544$ is the critical length for a catenoid in the absence of a field. In Section 4.1, we obtained an asymptotic approximation for σ^* when $\lambda << 1$, given by Equation (4.15). Physically, this can be interpreted to mean that the electric field is serving to stabilize the bridge at greater lengths than with zero voltage. A natural question to ask is, "What is the limit of this stabilization effect?" In other words, how far can we increase the critical length by increasing λ? Our goal in this section is to answer this question. To do so, we need to connect the phase plane analysis of Section 3 with the asymptotic results of Section 4.

We begin by examining the stability of the cylinder solution $u = 1$. In general, the requirement for stability is that the second variation of the functional $\mathcal{E}[u]$ be greater than zero. Physically, the surface will meet this criteria if it is stable subject to axially symmetric mechanical perturbations. As outlined in [4], the requirement that the second variation be greater than zero may be expressed in terms of conjugate points for a second order differential equation. In particular, we look at the solution $h(z)$ of the initial value problem

$$\begin{aligned} -\frac{d}{dz}(Ph') + Qh &= 0 \\ h(-1/2) = 0, \quad h'(-1/2) &= 1 \end{aligned} \tag{5.1}$$

where

$$P = \frac{\sigma^2 u}{2(1+\sigma^2 u'^2)^{3/2}}, \quad Q = \frac{1}{2}\left(\frac{\lambda(\ln(\delta/u) - 2)}{u^2 \ln^3(\delta/u)} - \frac{\sigma^2 u''}{(1+\sigma^2 u'^2)^{3/2}}\right). \tag{5.2}$$

If there are no points $c \in (-1/2, 1/2]$ such that $h(c) = 0$, then the functional $\mathcal{E}[u]$ given by Equation (2.5) has a weak minimum at the function $u(z)$. If such a c does exist, it is referred to as a conjugate point. This approach is only valid if $P > 0$; however, this will be true for any solution since all solutions satisfy $u > 0$.

In general, the functions P and Q given in Equation (5.2) are too complicated to allow for an analytic solution of the IVP of Equations (5.1), and alternate approaches to stability may be desirable. See [7] for a discussion on stability and the alternative "preferred coordinate" bifurcation diagram approach presented in [6]. For the cylinder solution $u = 1$, however, Equations (5.1) are greatly simplified. In this case, they become

$$\begin{aligned} h'' + \mu^2 h &= 0 \\ h(-1/2) = 0, \quad h'(-1/2) &= 1 \end{aligned} \tag{5.3}$$

where μ is given by Equation (4.18) is the same parameter as in Section 4.2. Solving the system (5.3), it is easily seen that there are no conjugate points only if $\mu < \pi$. This means that the cylinder solution is stable only in the range $\mu < \pi$.

To further explore the cylinder solution and the importance of the parameter μ, we place the cylinder solution and its perturbation in the phase plane. The cylinder solution occurs when $\lambda = \lambda_{cyl} = \ln^2 \delta$. When λ is close to but less than this value, there are two solutions that are "close" to being cylindrical. These solutions are found on opposite sides of the critical point $(u^*_{(2)}, 0)$, which satisfies $u^*_{(2)} > 1$. Hence one solution satisfies $u(0) < 1$, and one satisfies $u(0) > 1$. In terms of the phase plane,

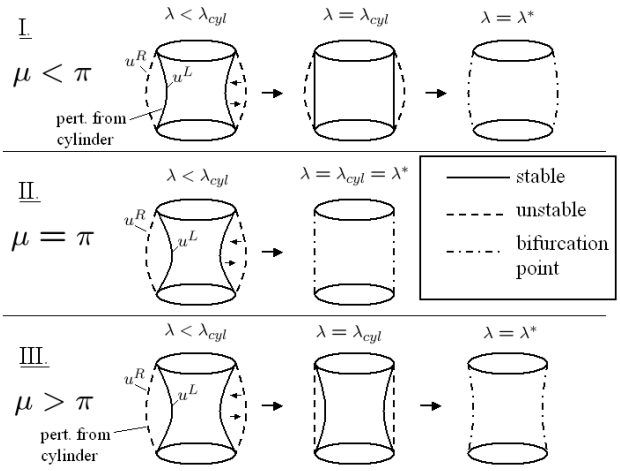

FIG. 5.1. *Stability of cylinder solution and dependence on the parameter* μ.

the former sits to the left of the line $u = 1$ and the latter sits to the right of $u = 1$. We refer to the former as u^L and the latter as u^R. When $\lambda = \lambda_{cyl}$, the critical point is on the line $u = 1$, and so the critical point itself represents a solution; namely, the cylindrical solution. One of the solutions u^L or u^R has become this solution. As we continue to increase λ, the critical point continues to move left, and the two solutions bifurcate at a critical value λ^*.

The details of this bifurcation and where the perturbation from the cylinder fits in depends entirely on the value of μ. We find [7] that when $\mu < \pi$, the bifurcation occurs on the right side of $u = 1$. Hence, a stable "bulge" of the cylinder is achievable. On the other hand, when $\mu > \pi$, the bifurcation occurs on the left side of $u = 1$, and so in this case a stable "bulge" of the cylinder is not achievable. In other words, the membrane becomes unstable before deflecting out to a cylindrical state.

If $\mu = \pi$, there are two symmetric solutions for $\lambda < \lambda_{cyl}$, but no solution when $\lambda > \lambda_{cyl}$. In this case, u^L and u^R each represent perturbations from the cylinder. Thus, at the stability boundary $\mu = \pi$, the bifurcation occurs right at λ_{cyl} and so there is no solution for $\lambda > \lambda_{cyl}$. These three cases and the solution profiles for u^L and u^R are depicted in Figure 5.1.

In Figure 5.2, we return to the full spiral meander described earlier, and mark the special solutions of the perturbations from the catenoid and the cylinder. For the cylinder perturbations, we indicate the solutions u^L and u^R described above. With regard to the catenoid perturbations, it is easily verified by a numerical solution of the ODE (5.1) that the perturbation of the stable catenoid is a stable solution, while the perturbation of the unstable catenoid is unstable.

As was just discussed, either u^L, u^R, or both can represent the perturbation from the cylinder, but u^L is always the stable solution. This same solution also represents the perturbation from the stable catenoid. There is a transition as the parameter λ is increased. For small enough λ, this solution will be given by the perturbation of the stable catenoid. As λ gets close to the cylinder voltage, though, the small voltage asymptotic analysis loses validity, and this solution transitions to the u^L cylinder solution.

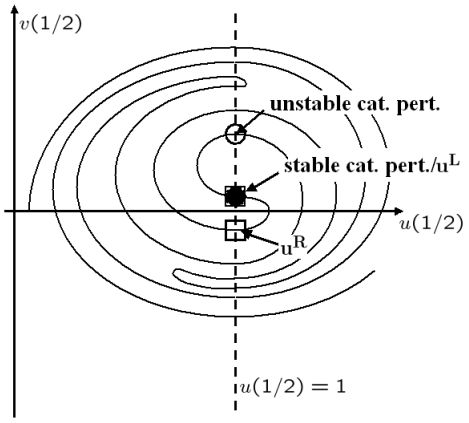

FIG. 5.2. *Special solutions in the spiral meander.*

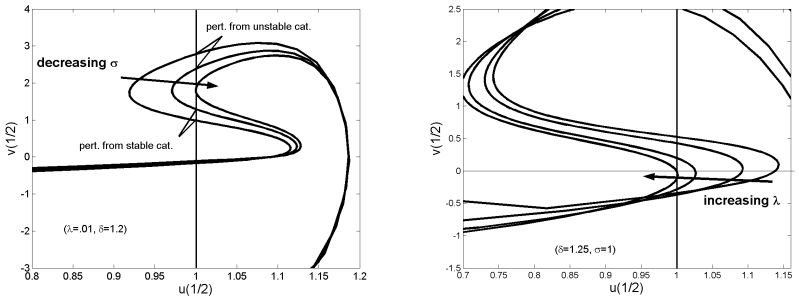

(a) (b)

FIG. 5.3. *(a) - The effect of decreasing σ in the meander plot. (b) - The effect of increasing λ in the meander plot.*

In terms of this spiral meander, decreasing σ causes the center part of the meander between the two catenoid perturbations to move to the right, until a bifurcation occurs at σ^*, corresponding to a critical length. In Figure 5.3(a), the evolution of this part of the meander curve is displayed. Likewise, when increasing λ, the curve moves left, causing the bifurcation between u^L and u^R at λ^*. This corresponds to a critical voltage. This evolution is displayed in Figure 5.3(b).

5.1. Critical length vs. critical voltage. For fixed λ and δ there is a critical value, σ^*, at which instability sets in, while for fixed σ and δ instability sets in at a critical value λ^*. In each case, the same stable solution, which we have denoted u^L, disappears, but the method of instability is quite different. Physically, σ^* represents reaching a critical length. When this length is reached, the membrane "pinches off" in the middle and forms two separated surfaces. On the other hand, λ^* denotes the well-known "pull-in" voltage of MEMS/NEMS [9]. When this critical value is reached, the electrostatic force dominates the elastic force in the system and the membrane collides with the electrode. For this geometry, we expect the instability that occurs at λ^* to be such that the membrane deflects outward until it hits the outer cylinder. Hence, the dynamics that occur at the onset of instability are very different in the

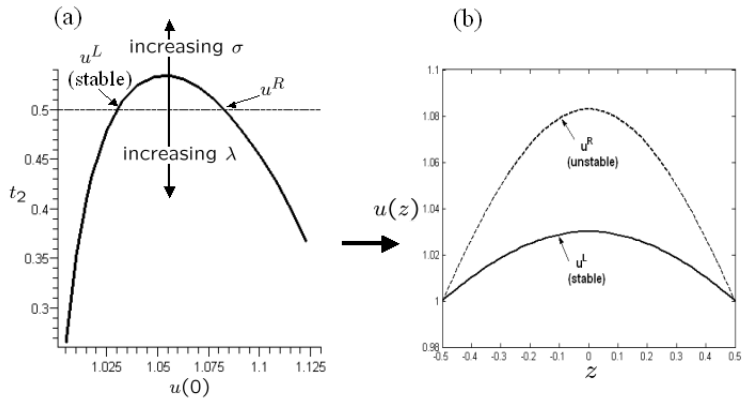

FIG. 5.4. *(a) - Plot of $t_2(u_0)$ for $\sigma = 2$, $\lambda = 0.05$ and $\delta = 1.2$. (b) - The resulting solution curves u^L and u^R.*

case of σ^* versus λ^*.

To determine the relationship between these two instabilities and to answer the question of the limit of the stabilization effect posed at the start of this section, we consider λ^* in greater detail. We have already seen that in the case of the cylindrical solution, the bifurcation between the two solutions denoted u^L and u^R occurs at $\lambda = \lambda_{cyl} = \ln^2 \delta$ when $\mu = \pi$. Hence in the special case $\mu = \pi$, we have that $\lambda^* = \ln^2 \delta$. Recall that $\mu^2 = (2 - \ln \delta)/(\sigma^2 \ln \delta)$. If we define $\hat{\sigma}$ by

$$\hat{\sigma}^2 = \frac{2 - \ln \delta}{\pi^2 \ln \delta} \,, \tag{5.4}$$

then in the $\sigma - \lambda$ plane, we know that λ^* will cross the point $\sigma = \hat{\sigma}$, $\lambda = \ln^2 \delta$. This point is the minimum value of λ^*, for as we have seen, in either case $\mu < \pi$ or $\mu > \pi$, the bifurcation between u^L and u^R occurs for $\lambda > \lambda_{cyl}$. To determine the behavior of λ^*, we consider separately the cases $\sigma > \hat{\sigma}$ and $\sigma < \hat{\sigma}$, or, equivalently, the cases $\mu < \pi$ and $\mu > \pi$ respectively.

For $\sigma > \hat{\sigma}$, $\mu < \pi$, and the bifurcation between u^L and u^R occurs to the right of the line $u = 1$. In other words, a stable bulge of the cylinder is seen. To understand the details of the bifurcation, we return to the phase plane and consider the time of flight from the u-axis to the line $u = 1$. Following the notation of Figure 3.3, we denote this by $t_2(u_0)$, $u_0 = u(0)$ where $u(0) > 1$. Note that trajectories outside the homoclinic orbit approach vertical asymptotes and that solutions will only be found in the region $u_0 < u_0^*$, where u_0^* is the trajectory bounded by $u = 1$ [7].

A sample curve for t_2 is given in Figure 5.4(a), where we observe the two solutions u^L and u^R as the points where $t_2 = 1/2$. The corresponding solutions are then plotted in Figure 5.4(b). We may write

$$t_2(u_0) = \sigma \int_1^{u_0} \frac{du}{\sqrt{\frac{u^2}{(u_0 + \lambda\Gamma)^2} - 1}}, \quad \Gamma := \frac{1}{\ln(\delta/u)} - \frac{1}{\ln(\delta/u_0)} \,. \tag{5.5}$$

Clearly, $\frac{\partial t_2}{\partial \sigma} > 0$. Also, it is shown in [7] that $\frac{\partial t_2}{\partial \lambda} < 0$ in the relevant region $1 < u_0 < u_0^*$. This implies that an increase in λ causes the two solutions to bifurcate as

expected, while increasing σ causes the opposite to occur: t_2 increases, so that the curve moves upward. Hence, the shorter the bridge, the more voltage may be applied while keeping a stable solution. Increasing σ will not cause a critical value to be reached, and so there is no limit to the effect. For any value of λ, we may find a value of σ for which the peak of t_2 is above the line $t_2 = 1/2$. Hence, as $\sigma \to \infty$, $\lambda^* \to \infty$. This result is interesting in the context of the phase plane. As λ is increased, a value is reached independently of σ at which the homoclinic orbit is entirely to the left of the line $u = 1$ [7], at which point no solutions can be found inside the homoclinic orbit. However, the stable solution u^L simply crosses over the homoclinic orbit and remains. Further, as was noted in Section 3, for $\lambda > 4\delta/e^2$, there are no critical points in the system, the spiral structure of the meander is completely lost, and yet still a stable solution to the problem persists. One way to think of this physically is that as $\sigma \to \infty$, the surface area of the membrane becomes infinitesimally small, and so there is nothing for the electric field to "pull" on, and thus infinite voltage is required to bring about instability. Keep in mind, however, that in taking σ to infinity, we quickly violate the asymptotic assumption $\epsilon^2 << 1$. Thus, our analysis is not suited to make concrete physical conclusions for large σ.

Next, we consider the case $\mu > \pi$. Suppose that $\lambda \in (\ln^2 \delta, \lambda^*)$ and $\sigma < \hat{\sigma}$. Then $\mu > \pi$, which implies that the bifurcation at λ^* will occur to the left of the line $u = 1$. Before the bifurcation, the three monotonic solutions u^L, u^R, and the perturbation from the unstable catenoid (see Figure 5.2) are all located to the left of the critical point $u^*_{(2)}$, which satisfies $u^*_{(2)} < 1$ because $\lambda > \ln^2 \delta$. For convenience, we refer to the perturbed unstable catenoid solution as u^C. We have then one stable solution, u^L, flanked by two unstable solutions, u^R to the right and u^C to the left. Since they are all monotonic, the curve $t_1(u_0)$ will intersect the line $t_1 = 1/2$ three times. From Equation (3.8), we may write

$$t_1(u_0) = \sigma \int_{u_0}^{1} \frac{du}{\sqrt{\frac{u^2}{(u_0+\lambda\Gamma)^2} - 1}}, \quad \Gamma := \frac{1}{\ln(\delta/u)} - \frac{1}{\ln(\delta/u_0)} \, . \tag{5.6}$$

Taking a derivative with respect to λ, we have

$$\frac{\partial t_1}{\partial \lambda} = \sigma \int_{u_0}^{1} \left(\frac{u^2}{(u_0 + \lambda\Gamma)^2} - 1 \right)^{-3/2} \frac{u^2 \Gamma}{(u_0 + \lambda\Gamma)^3} \, du \, . \tag{5.7}$$

Since $u_0 < u < 1$ in the region of integration, $\Gamma > 0$, and so $\frac{\partial t_1}{\partial \lambda} > 0$. Hence, by increasing λ, the curve moves in the positive t_1 direction, causing a bifurcation between u^L and u^R once λ^* is reached. Also, it is clear that $\frac{\partial t_1}{\partial \sigma} > 0$, so decreasing σ will cause the curve to move downward and bring a bifurcation between u^L and u^C at σ^*. If, however, an increase in λ is countered by a decrease in σ, the two effects can be balanced so that the stable solution u^L remains. Physically, the situation is as follows. Increasing the voltage eventually pulls the membrane to the outer cylinder. Increasing the length causes surface tension to become too great for the bridge to sustain itself, and the membrane eventually collapses in on itself and pinches off. By increasing the voltage and the length together in the right proportions, the "pulling out" and the "pinching in" may be balanced so that the membrane remains stable.

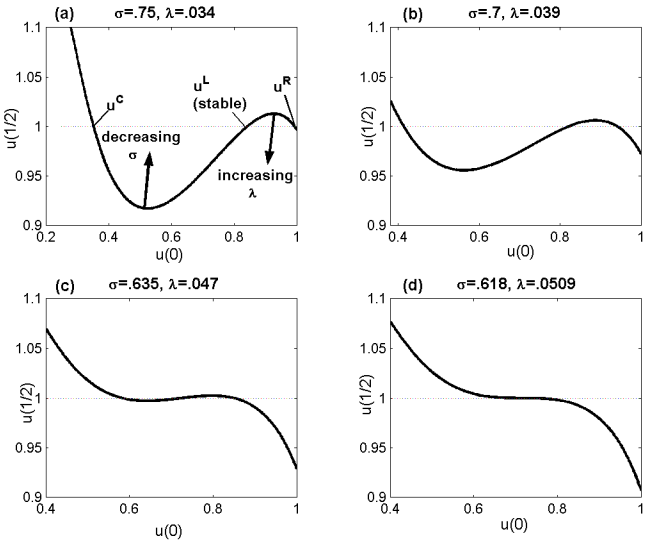

FIG. 5.5. *Progression of the curve $u(1/2)$ versus $u(0)$ as λ is increased and σ is decreased (and $\delta = 1.2$). The parameters are altered so that the stable solution u^L remains, but at each step, the middle portion of the curve flattens out. As is seen in (d), the three solutions coalesce and the stable solution is lost at a critical λ-σ pair.*

We now ask whether there is a bound to this balancing effect. To answer this, we consider the plot of $u(1/2)$ versus $u(0)$, produced by iterating through different values of $u(0)$, integrating the ODE forward for $1/2$, and plotting $u(1/2)$ as a function of $u(0)$. Any intersection with the line $u(1/2) = 1$ gives a solution to the problem. Qualitatively, this will produce a curve equivalent to considering $t_1(u_0)$, but is easier to produce numerically and so is used here. Note that by construction, the meander plot will behave in the exact opposite way as $t_1(u_0)$ as λ and σ are altered, so that the curve will move up as σ is decreased and down as λ is increased. In any case, the qualitative characteristics of the bifurcation are just as evident, and we are in a position to determine the limit of the balancing effect of λ and σ.

In Figure 5.5, the meander curve $u(1/2)$ is plotted as a function of $u(0)$ for varying values of σ and λ for $\delta = 1.2$ fixed. As we follow the sequence of pictures, σ is decreased while λ is increased. This balancing of the two parameters enables the stable solution u^L to remain. However, the curve flattens out as we do this, so that in Figure 5.5(d) the three solutions have collided into one. At this critical $(\sigma,\ \lambda)$ pair, σ^* has intersected λ^*. This is really quite remarkable. Physically, it appears that if the length and the voltage are balanced in such a way that the bridge remains stable, a point is reached at which the pull-in voltage and the critical length occur simultaneously! This raises interesting dynamics questions of what in fact the membrane will do and in which direction the instability will cause the membrane to move. We leave the answers to these questions for future work, and for the moment merely mention the end result that there is indeed a limit to the balancing of voltage and length, and it occurs at the intersection of the stability boundaries σ^* and λ^*.

The general shape of $\sigma^*(\lambda)$ and $\lambda^*(\sigma)$ is now complete. A numerically produced example is provided in Figures 5.6 and 5.7 for the value $\delta = 1.2$. Figure 5.6 shows a

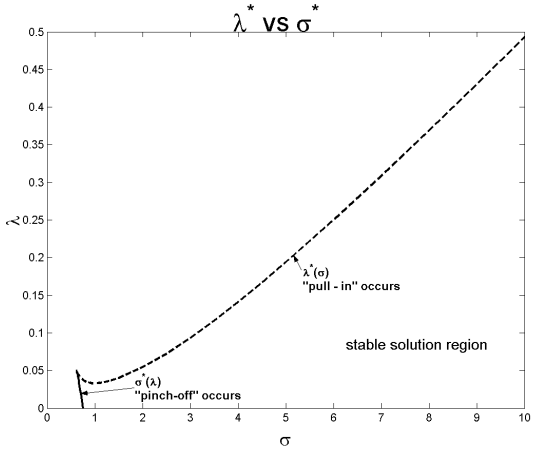

FIG. 5.6. *Plot of $\sigma^*(\lambda)$ vs $\lambda^*(\sigma)$. The behavior of λ^* for large σ is evident. Here $\delta = 1.2$*

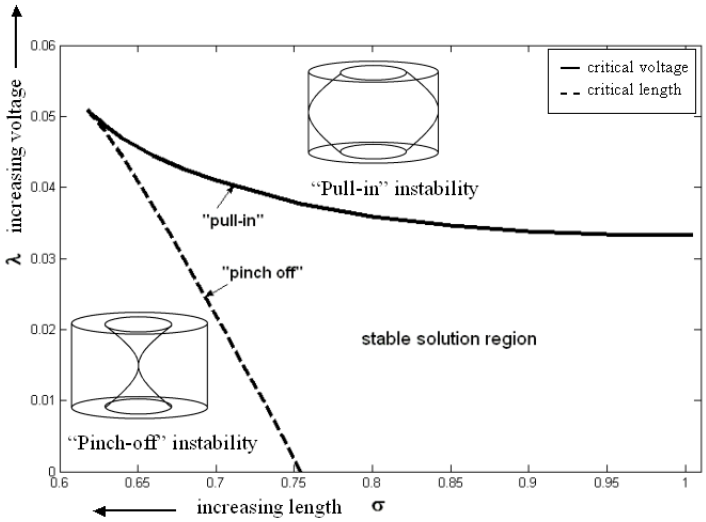

FIG. 5.7. *Plot of $\sigma^*(\lambda)$ vs $\lambda^*(\sigma)$, zoomed in on the region where σ^* and λ^* intersect. Stable solutions exist inside the two curves. The type of instability that occurs at each boundary is illustrated. Here $\delta = 1.2$*

larger region to see more generally the structure of these two curves. As mentioned earlier, keep in mind that larger values of σ violate the asymptotic assumption $\epsilon^2 << 1$, and so the right side of the curve in Figure 5.6 may not be physically relevant. The more interesting aspect of these curves occurs for values of σ that do fall in the relevant range, though. Figure 5.7 shows this region more closely, zoomed in on the intersection of λ^* and σ^*.

6. Conclusion. In this paper, we have explored the equilibrium solutions of a catenoid bridge under the influence of an axially symmetric applied electric field. We began by formulating the mathematical model, arriving at the governing differential

equation through minimization of an energy functional. From there, our objective was to analyze the resulting boundary value problem. We began by using standard techniques from the theory of dynamical systems. We uncovered a rich structure to the solution set, illustrated by Figure 3.4. Our second approach to understanding the boundary value problem was to use perturbation methods to study various limiting situations. This allowed us to find approximate solutions and also to determine the relationship between key parameters in the problem.

One important technological question addressed in this work is whether or not the electric field allows for significant manipulation of the surface. One clear result attained here is that the field may be used to stabilize structures that would otherwise be unstable. We first saw this in the case of the perturbed catenoids, where the bifurcation between the stable and unstable catenoids occurred at a greater length than in the case of zero voltage. We further explored this by considering the relationship between critical length and critical voltage. Physically, the stabilization occurs because the electric field is applied to counteract the surface tension force in the system. We have shown that these forces can be balanced in interesting ways, leading to structured surfaces unobtainable without an electric field. We also found the intersection of the two different instabilities corresponding to critical length and critical voltage. This intersection poses an interesting dynamical dilemma which warrants further analysis.

More generally, we have begun an exploration of Field Driven Mean Curvature (FDMC) surfaces; that is, membranes whose shape in the absence of external forces minimizes surface area, that are placed in an applied field. In a sense, this brings together two areas – electrostatic actuation and mean curvature surfaces. The study of such surfaces is potentially applicable in a host of fields, from MEMS and NEMS devices to liquid control in low gravity environments to the emerging field of self-assembly.

REFERENCES

[1] P. Concus, R. Finn, and J. McCuan, *Liquid bridges, edge blobs, and Scherk-type capillary surfaces*, Indiana Univ. Math. J. 50 (2001), pp. 411-441.

[2] B. Fiedler, *Realization of Meander Permutations by Boundary Value Problems*, J. Diff. Eq., 156 (1999), pp. 282-308.

[3] G. Flores, G. Mercado, and J.A. Pelesko, *Dynamics and Touchdown in Electrostatic MEMS*, in Proceedings of Design Engineering Technical Conferences, ASME, Chicago, IL, 2003.

[4] I.M. Gelfand and S.V. Fomin, *Calculus of Variations*, Dover, Mineola, New York, 1963.

[5] E. Kim and G.M. Whitesides, *Use of Minimal Free Energy and Self-Assembly to Form Shapes*, Chem. Mater. 7 (1995), pp. 1257-1264.

[6] J.H. Maddocks, *Stability and Folds*, ARMA 99 (1987), pp. 301-308.

[7] D.E. Moulton, *Mathematical Modeling of Field Driven Mean Curvature Surfaces*, Ph.D. dissertation, University of Delaware (2008).

[8] S. Paruchuri and M.P. Brenner, *Splitting a Liquid Jet*, Phys. Rev. Lett. 98 (2007), 134502.

[9] J.A. Pelesko and D. Bernstein, *Modeling MEMS and NEMS*, Chapman Hall and CRC Press, (2002).

[10] J. Plateau, *Statique Expérimentale et Théoretique des Liquides*, Gautier-Villars, Paris, 1873. 377-401

[11] S. Strogatz, *Nonlinear Dynamics and Chaos*, Perseus Books, Cambridge, MA, 1994.

[12] G.I. Taylor, *The Coalescence of Closely Spaced Drops when they are at Different Electric Potentials*, Proc. Roy. Soc. A 306 (1968), pp. 423-434.

[13] R. Weinstock. *Calculus of Variations, with Applications to Physics and Engineering*, Dover, New York, 1974.